


Bisphenol S and Epidermal Growth Factor Receptor Signaling in Human Placental Cytotrophoblasts

Elvis Ticiani,¹ Jeremy Gingrich,² Yong Pu,¹ Mathew Vettathu,³ Jacquelyn Davis,³ Denny Martin,³ Margaret G. Petroff,^{4,5} and Almudena Veiga-Lopez¹ 

¹Department of Pathology, University of Illinois at Chicago, Chicago, Illinois, USA

²Department of Pharmacology and Toxicology, Michigan State University (MSU), East Lansing, Michigan, USA

³Sparrow Health System, Lansing, Michigan, USA

⁴Department of Pathobiology and Diagnostic Investigation, MSU, East Lansing, Michigan, USA

⁵Department of Microbiology and Molecular Genetics, MSU, East Lansing, Michigan, USA

BACKGROUND: Bisphenol S (BPS) is an endocrine-disrupting chemical and the second most abundant bisphenol detected in humans. *In vivo* BPS exposure leads to reduced binucleate cell number in the ovine placenta. Binucleate cells form by cellular fusion, similar to the human placental syncytiotrophoblast layer. Given that human placental syncytialization can be stimulated through epidermal growth factor (EGF), we hypothesized that BPS would reduce human cytotrophoblast syncytialization through disruption of EGF receptor (EGFR) signaling.

OBJECTIVE: We tested whether BPS interferes EGFR signaling and disrupts human cytotrophoblast syncytialization.

METHODS: We first tested BPS competition for EGFR using an EGF/EGFR AlphaLISA assay. Using human primary term cytotrophoblast cells (hCTBs) and MDA-MD-231 cells, a breast cancer cell line with high EGFR expression, we evaluated EGFR downstream signaling and tested whether BPS could inhibit the EGF response by blocking EGFR activation. We also evaluated functional end points of EGFR signaling, including EGF endocytosis, cell proliferation, and syncytialization.

RESULTS: BPS blocked EGF binding in a dose-dependent manner and reduced EGF-mediated phosphorylated EGFR in both cell types. We further confirmed that BPS acted as an EGFR antagonist as shown by a reduction in EGF internalization in both hCTBs and MDA-MD-231 cells. Finally, we demonstrated that BPS interfered with EGF-mediated cell processes, such as cell proliferation in MDA-MD-231 cells and syncytialization in hCTBs. EGF-mediated, but not spontaneous, hCTB syncytialization was fully blocked by BPS (200 ng/mL), a dose within urinary BPS concentrations detected in humans.

CONCLUSIONS: Given the role of EGFR in trophoblast proliferation and differentiation during placental development, this study suggests that exposures to BPS at environmentally relevant concentrations may result in placenta dysfunction, affecting fetal growth and development. <https://doi.org/10.1289/EHP7297>

Introduction

A variety of structurally diverse compounds classified as endocrine-disrupting chemicals (EDCs) have been reported to affect the endocrine system through direct receptor binding or through alternative pathways that can inhibit or stimulate the production or modulate the activity of hormones (Diamanti-Kandarakis et al. 2009). Used in the production of plastics and the manufacturing of consumer products, bisphenols are high-production volume chemicals (U.S. EPA 2016) and among the most prevalent EDCs worldwide (Gore et al. 2015). After bisphenol A (BPA), bisphenol S (4,4'-sulfonyldiphenol; BPS) is the second most abundant bisphenol congener detected in humans, being found in over 80% of human urine samples from the United States, China, Japan, and Vietnam (Liao et al. 2012a). BPS can be found in foodstuffs (Liao and Kannan 2013), indoor dust (Liao et al. 2012b), sewage sludge (Yu et al. 2015), thermal receipt paper (Rocha et al. 2015), groundwater (Yamazaki et al. 2015), and sediments from industrialized areas (Liao et al. 2012c). Notably, BPS is being used as a replacement for BPA in thermal paper manufacturing (ECHA 2020).

Previous studies have demonstrated that even at low exposure doses, BPS can alter neurodevelopment (Kinch et al. 2015) and the reproductive endocrine system (Qiu et al. 2016) in fish. In mice, BPS has increased estrogen-responsive gene expression in the ovary and uterus, interfering in the development of the reproductive tract (Hill et al. 2017). In sheep, gestational exposure to BPS, but not BPA, reduced maternal circulating pregnancy-associated glycoproteins due to a reduction in the number of binucleate cells, which are analogous to syncytialized human cytotrophoblasts (hCTBs) in the placenta (Gingrich et al. 2018). These placentas also had ~50% lower e-cadherin protein expression and reduced expression of genes involved in trophoblast cell fusion [envelop Jaagsiekte sheep retrovirus (*enJSRV*) and hyaluronoglucosaminidase 2 (*HYAL2*)] leading to binucleate cell formation (Gingrich et al. 2018). Altogether, these findings point to a compromise in hormone and glycoprotein placental production stemming from a loss in binucleated cells. However, the mechanism underlying BPS-induced placental dysfunction remains unknown.

The placenta is the interface between the fetus and the mother, plays a key role in fetal growth by regulating hormone synthesis and nutrient transport (Fowden and Moore 2012), and is composed of multiple cell types, including macrophages, cytotrophoblasts, stromal cells, and endometrial cells (Wong and Cox 2017). In humans, as placental development progresses, cytotrophoblasts differentiate into two distinct cell populations: a) extravillous cytotrophoblasts, which proliferate and invade the uterine wall and are important for remodeling the endometrial vasculature; and b) syncytiotrophoblasts (STBs), which arise as a result of cytotrophoblast fusion and are responsible for the endocrine function of the placenta by secreting hormones, including progesterone, chorionic gonadotropin, and placental lactogen (Malassiné and Cronier 2002). Epidermal growth factor (EGF) is required for proper control of cytotrophoblast growth and differentiation into STBs (Dackor et al. 2007; Filla and Kaul 1997). It has been hypothesized

Address correspondence to Almudena Veiga-Lopez, Department of Pathology, University of Illinois at Chicago, 909 S. Wolcott Ave., Room 6093, Chicago, IL 60612 USA. Email: veiga@uic.edu

Supplemental Material is available online (<https://doi.org/10.1289/EHP7297>).

The authors declare they have no actual or potential competing financial interests.

Received 22 April 2020; Accepted 21 January 2021; Published 19 February 2021.

Note to readers with disabilities: *EHP* strives to ensure that all journal content is accessible to all readers. However, some figures and Supplemental Material published in *EHP* articles may not conform to 508 standards due to the complexity of the information being presented. If you need assistance accessing journal content, please contact ehponline@niehs.nih.gov. Our staff will work with you to assess and meet your accessibility needs within 3 working days.

that EGF exerts a gestational age-dependent action on the placenta, by stimulating cytotrophoblast proliferation in early pregnancy (4–5 wk) and stimulating differentiation into STBs later in pregnancy (Maruo et al. 1992; Seravalli et al. 2020). Consistent with the importance of EGF receptor (EGFR) signaling during placental development, EGFR has the highest expression in the human placenta compared with all non-tumorigenic (Uhlén et al. 2015). Importantly, altered EGFR expression is associated with placental pathologies, such as intrauterine growth restriction, preeclampsia, and placenta accreta (Faxén et al. 1998; Tseng et al. 2004).

The syncytialization process that occurs in the human placenta can be reproduced *in vitro* by using purified cytotrophoblasts (Fujii et al. 2017), which aggregate and spontaneously fuse to form STBs. This cellular fusion process can be enhanced by EGF exposure (Kliman et al. 1986). Given that BPS reduces binucleate cell number in the ovine epitheliochorial placenta (Gingrich et al. 2018), that binucleate trophoblast cells form in a similar process to that of human STBs, and that human placental syncytialization can be induced through EGF/EGFR stimulation, we hypothesized that BPS interferes with hCTB syncytialization through disruption of EGFR signaling. To test whether BPS can impair cytotrophoblast syncytialization in the human hemochorial placenta through EGFR antagonism, we used a combination of approaches, including a competitive binding assay, gene and protein expression, and EGF endocytosis assays in cells with high EGFR expression, including primary hCTBs.

Methods

Exposure Chemicals

Chemicals used in this study were BPS (4,4-sulfonyldiphenol; Cat. No. 80-09-11; AcrosOrganics) and dimethylsulfoxide 114 (DMSO; Cat. No. BP231-100; ThermoFisher). The following forms of EGF were used: human EGF (Cat. No. E9644; Sigma-Aldrich) and AlexaFluor647-conjugated EGF (biotinylated EGF complexed to Alexa Fluor 647 streptavidin; Cat. No. E13345; ThermoScientific).

EGF/EGFR Competitive Binding Assay

To evaluate the capacity of BPS to block EGFR, an AlphaLISA EGF/EGFR binding kit (Cat. No. AL366HV; PerkinElmer) was used per the manufacturer's recommendation. In brief, anti-human IgG Fc-specific AlphaLISA acceptor beads and EGFR-Fc were mixed, incubated, and added to each well containing 0.0001, 0.001, 0.01, 0.1, 1.0, or 10 $\mu\text{g}/\text{mL}$ (or 0.0004, 0.0039, 0.039, 0.399, 3.99, and 39.95 μM of BPS, respectively) with biotinylated EGF ($n = 5$). The antibodies anti-EGF (Cat. No. MAB236; R&D Systems) and cetuximab (anti-EGFR; Cat. No. A2000; Selleck Chemicals LLC) at a dose of 0.1 $\mu\text{g}/\text{mL}$ were used as negative controls. Streptavidin-coated donor beads were then added to each well for quantification. The binding signal in alpha units from each well was measured at 615 nm using the AlphaLISA mode on a microplate fluorometer (Synergy Neo; BioTek). The half-maximal effective concentration (EC_{50}) was calculated using GraphPad Prism 8 (GraphPad Software, Inc.).

hCTB Cell Isolation, Purification, and Syncytialization

Healthy placentas derived from elective C-section term pregnancies ($n = 6$) were collected after written informed consent [institutional review board (IRB) approval of Sparrow Health System and Michigan State University (IRB No. 15-484M)]. hCTB cells were then isolated as previously described (Petroff et al. 2006). Subjects were enrolled considering the following exclusion criteria: fetal developmental abnormalities, multiple pregnancies, maternal

diagnosis of human immunodeficiency virus, hepatitis B or C, polycystic ovary syndrome, or congenital adrenal hyperplasia. Placental tissue was first rinsed with 0.9% sodium chloride and then transferred to a 150-mm petri dish. After gently mincing with scissors, the villous tissue was dissociated with an enzyme digestion solution [25 mM (4-(2-hydroxyethyl)-1-piperazineethanesulfonic acid) HEPES, 2.5% trypsin, and ~ 300 Kunitz U/mL DNase (Cat. No. 15090-046; Gibco) in Hank's balanced salt solution]. The resulting cell suspension was then collected, layered on fetal bovine serum (FBS; Cat. No. 35-010-CV; Corning), and centrifuged. The cell pellet was resuspended in Iscove's modified Dulbecco's medium (IMD; Cat. No. I3390; MilliporeSigma). Cell suspensions were filtered through a 100- μm nylon cell strainer, followed by a Percoll gradient centrifugation. The visible cell band between 30–50% Percoll was collected and resuspended in IMD medium supplemented with 10% FBS. To confirm cytotrophoblast cell characterization, the same method described in the immunocytochemistry section was performed using cytokeratin-7 (anti-cytokeratin 7; Cat. No. AB150116; Abcam) followed by goat anti-mouse Alexa Fluor 594 secondary antibody (Cat. No. A11001; Thermo Scientific) (Figure S1A). This method yielded $\sim 98\%$ cytotrophoblast cell purity when using an antibody against cytokeratin-7, through flow cytometry (Figure S1B), as previously described by Pötgens et al. (2001), hCTBs were targeted with a direct method using an Alexa Fluor 488-conjugated anti-CKT7 antibody (recombinant Alexa Fluor 488 anti-cytokeratin 7; Cat. No. AB185048; Abcam). Fluorescence was measured in channel FL1 and plotted in histograms. IgG control primary antibodies that lack specificity to the target were used as negative controls. Percentages of positive cells were corrected for control values. After isolation, cells were then stored in liquid nitrogen until needed. Each of the six hCTB primary cell cultures were seeded into a 24-well culture dish at a density of 1×10^6 cells/well. hCTBs were cultured overnight to allow cell attachment and then washed the following day with IMD medium to remove unattached cells. Each one of the six primary cell cultures were then exposed to four different culture conditions: *a*) vehicle, *b*) BPS (200 ng/mL), *c*) EGF (5 ng/mL), and *d*) BPS + EGF. EGF supplementation was used to enhance syncytialization, as previously described (Holets et al. 2009). DMSO was used as the vehicle group and added to a final concentration of 0.1% in all exposure groups. Exposure medium was replaced every 48 h for 96 h to evaluate syncytialization.

Cell Viability

Cell viability was determined using a thiazolyl blue tetrazolium bromide [3-(4,5-dimethylthiazol-2-yl)-2,5-diphenyltetrazolium bromide (MTT)] assay as previously described (Pu et al. 2019). hCTB cells were seeded into 96-well plates (100,000 cells/well) and cultured overnight in IMD medium to allow cell attachment. Cells were washed the following day to remove unattached cells and treated for 96 h with a range of BPS concentrations (0, 10, 100, 1,000, and 10,000 ng/mL) and as well in a combination of 1,000 ng/mL of BPS with 10 ng/mL of EGF or EGF alone ($n = 5$). Thereafter, the medium was replaced with 100 μL of phenol red-free MTT working solution (50 $\mu\text{g}/\text{mL}$) and incubated for 4 h. The MTT working solution was discarded and 100 μL of DMSO added into each well. Plates were vortexed for 10 min at room temperature and cell viability determined by absorbance quantification at 570 nm using a microplate reader (SpectraMax M5e; Molecular Devices LLC).

Immunocytochemistry

Following hCTB syncytialization (96 h), cells were fixed using a 1:1 methanol:acetone solution at -20°C for 20 min, followed by

three tris-buffered saline (TBS) washes, and subjected to immunocytochemical staining. Fixed cells were blocked with 5% bovine serum albumin in TBS containing 0.03% Tween-20 (TBS-T; blocking buffer). Anti-desmoplakin primary antibody (Cat. No. AB16434; Abcam) was diluted at a concentration of 1:200 in blocking buffer, and the cells were exposed overnight at 4°C. Thereafter, cells were incubated for 1 h at room temperature in goat anti-mouse Alexa Fluor 488 secondary antibody (Cat. No. A11001; Thermo Scientific) at a concentration of 1:1,000 diluted in blocking buffer. Cells were then stained with 4',6-diamidino-2-phenylindole (DAPI; 1:1,000) to identify the nuclei. Negative control groups are presented in Figure S1C. All exposure groups were imaged using an Olympus BX41 microscope (Olympus) with an Olympus DP71 camera or a Leica DMLB microscope (Leica) with a Leica DFC480 camera. Ten random images per well were captured at 20× magnification for quantification of syncytia. A syncytia was defined as a cluster of three or more nuclei per continuous desmoplakin-stained border. An average [\pm standard deviation (SD)] of 962 ± 41 nuclei was counted per treatment. The number of syncytia per image were quantified and normalized to the total number of nuclei to determine proportion of syncytialized cells and normalized to the spontaneous vehicle control group for each primary cell line tested.

MDA-MD-231 Cell Culture and Proliferation

We further tested the ability of BPS to interfere with EGFR using MDA-MD-231 human breast cancer cells (Cat. No. 92020424; Sigma-Aldrich). MDA-MD-231 cells are triple-negative breast cancer cells (i.e., they lack estrogen, progesterone, and receptor tyrosine-protein kinase erbB-2), have high EGFR expression, and proliferate in response to EGF. This makes them highly suitable for mechanistic studies (Yu et al. 2018; Kang et al. 2018). MDA-MD-231 cells were maintained in Dulbecco's modified Eagle's medium/F12 medium (Cat. No. 124000-024; MilliporeSigma) supplemented with 10% FBS, 2 mM L-glutamine, 10 mM HEPES, 100 IU/mL penicillin, and 100 μ g/mL streptomycin. Cells were cultured in 5% carbon dioxide CO₂ at 37°C. MDA-MD-231 cell proliferation was determined using a 5-ethynyl-2'-deoxyuridine (EdU) cell proliferation assay kit (EdU-488; Cat. No. 17-10525; Millipore, Sigma-Aldrich), as previously described (Jing et al. 2019). In brief, MDA-MD-231 cells were cultured in growth medium in a 24-well plate and at 20% of confluence, exposed in triplicate to four different culture conditions: vehicle, BPS (1,000 ng/mL), EGF (10 ng/mL), and BPS + EGF (1,000 ng/ml BPS + 10 ng/ml EGF). DMSO was used as the vehicle group and added to a final concentration of 0.1% in all exposure groups. After 72 h, the medium was replaced with 10 mM EdU solution in growth medium for 3 h at 37°C and 5% CO₂. Cells were then fixed and stained with DAPI (1:1,000). Twelve non-overlapping images were captured from each well using a fluorescence microscope (Lioheart FX; Biotek). The percentage of proliferating cells was defined as the percentage of EdU-positive nuclei to total DAPI-stained nuclei.

EGF Endocytosis Assay

EGF internalization was evaluated in MDA-MD-231 and hCTBs using a modified EGF endocytosis assay (Hardesty et al. 2018). Cells were seeded in 12-well plates, and after they reached 80% of confluency, the cells were serum starved overnight and pretreated with BPS (1 or 10 μ g/mL) in 0.1% of DMSO for 5 min, followed by a 5 min co-exposure with BPS (1 and 10 μ g/mL) and Alexa Fluor 647-conjugated EGF (100 ng/mL, biotinylated EGF complexed to Alexa Fluor 647 streptavidin). The positive control group was exposed to 0.1% of DMSO and each treatment was run in triplicate. Negative controls were treated with 100 ng/mL unlabeled

recombinant human EGF. The cells were then washed with pre-warmed phosphate-buffered saline and incubated at 37°C in serum-free IMD medium for 60 min. The cells were next fixed using a 1:1 methanol:acetone solution at -20°C for 20 min, followed by three TBS washes, and immunostained overnight for phosphorylated EGFR (p-EGFR) using the primary antibody antiphospho-EGFR (Cat. No. 3777; Cell Signaling). Thereafter, the cells were incubated for 1 h at room temperature in goat anti-mouse Alexa Fluor 488 secondary antibody (Cat. No. A11001; Thermo Scientific) at a concentration of 1:1,000 diluted in blocking buffer. Cell nuclei were stained with Hoechst 33342 (10 μ g/mL; Cat. No. 94403; Sigma-Aldrich). For quantification of EGF endocytosis and p-EGFR, three random images (40× magnification) per well for a total of three wells per treatment group were obtained using an Olympus BX41 fluorescence microscope and Olympus DP71 camera. Filter sets for 350, 488, and 647 nm were used for detection of Hoechst, p-EGFR, and Alexa Fluor 647-conjugated EGF, respectively. Cells (mean \pm SD: $1,800 \pm 152$ per group) from randomized fields from each group were analyzed using the CellProfiler software (McQuin et al. 2018). Total labeled EGF was normalized to the number of nuclei. For additional details on chemical sources, see the section "Exposure Chemicals."

Western Blotting

MDA-MD-231 cells were cultured in growth medium in a 6-well plate and exposed in triplicate to four different culture conditions: vehicle, BPS (1,000 ng/mL), EGF (10 ng/mL), and BPS + EGF (1,000 ng/ml BPS + 10 ng/ml EGF). DMSO was used as the vehicle group and added to a final concentration of 0.1% in all exposure groups. Cells were exposed for 15 min to enable evaluation of phosphorylated EGFR. After exposure, cells were harvested and protein extraction was performed using radioimmunoprecipitation assay lysis buffer (Cat. No. N653; VWR Life Science) containing 20% 1 M sodium fluoride, 1 mM sodium orthovanadate, and 1% protease inhibitor cocktail (Cat. No. M221; VWR Life Science). Protein concentration was determined using a Pierce bicinchoninic acid protein assay kit (Cat. No. 23225; Thermo Fisher). Twenty micrograms of protein per sample from cell lysates were subjected to electrophoresis on a 10% sodium dodecyl sulfate-polyacrylamide gel (120 V for 60 min). Protein was then transferred from the gel onto a nitrocellulose membrane (200 mA for 90 min) and subjected to western blotting. In brief, membranes were blocked with 5% nonfat dry milk in TBS containing 0.03% TBS-T and incubated with primary antibodies diluted in block overnight at 4°C. Primary antibodies used were anti-EGFR, anti-extracellular signal-regulated kinase (anti-ERK; Cat. Nos. AB32077 and AB17942, respectively; Abcam), anti- β -actin (Cat. No. A1978; MilliporeSigma), anti-protein kinase B (anti-AKT), antiphospho-Akt (Tyr 204), antiphospho-EGFR (Tyr 1068), and anti-phospho-p44/42 mitogen-activated protein kinase (MAPK; Thr202/Tyr204) (Cat. Nos. 9272S, 9271S, 3777S, and 4370S, respectively; Cell Signaling). After three TBS-T washes, membranes were incubated with horseradish peroxidase (HRP)-conjugated secondary antibodies goat anti-mouse HRP-conjugated and goat anti-rabbit HRP-conjugated (Cat. Nos. 115-005-003 and 111-005-003, respectively; Jackson ImmunoResearch) diluted 1:5,000 in block for 1 h at room temperature in the dark. Western Bright ECL (Enhanced Chemiluminescence) (Cat. No. K12045; Advanta) was used for enhanced chemiluminescence and visualized on a Thermo Scientific MYECL Imager (Thermo Scientific). Quantification of band intensities was performed using ImageJ software (Schneider et al. 2012). Differences in protein loading were accounted for by normalizing the target protein band by the control β -actin band for each sample.

Gene Expression

MDA-MD-231 cells were cultured in growth medium in a 12-well plate and exposed in triplicate to vehicle (0.1% DMSO), BPS (1,000 ng/mL), EGF (10 ng/mL), and BPS + EGF. After 3 h, cells were harvested and total RNA was extracted using an RNeasy Mini kit (Qiagen) following the manufacturer's protocol. RNA quality and concentration were measured by Nanodrop (Thermo Fisher Scientific). A total of 1 µg RNA (A260/A280: 2.0 ± 0.05, RNA concentration: 150 ± 50 ng/µL) was reverse transcribed into complementary DNA (cDNA) using a high-capacity cDNA reverse transcription kit (Promega) in 20 µL reaction volumes. Quantitative real-time polymerase chain reaction (qRT-PCR; QuantStudio 5; Thermo Fisher Scientific) was performed to quantify expression of genes responsive to EGFR: cyclin D1 (*CCND1*), prostaglandin-endoperoxide synthase (*PTGS2*), and MYC proto-oncogene (*MYC*). Primer sequences used for the SYBR green real-time qRT-PCR are shown in Table S1. Expression levels for indicated genes were calculated using the $\Delta\Delta CT$ method, normalized against glyceraldehyde 3-phosphate dehydrogenase (*GAPDH*), and presented as relative fold-change to that of the control. All experiments and qRT-PCR assays were run in triplicate. The cDNA amplification reaction (50 ng) consisted of template denaturation and polymerase activation at 95°C for 30 s, followed by 40 cycles of denaturation at 95°C for 15 s, annealing at 60°C for 30 s, and extension at 72°C for 30 s. Melt curve analyses were performed for all genes, and the specificity and integrity of the PCR products were confirmed by the presence of a single peak melt curve.

Statistical Analysis

Quantitative data comprising the proportion of syncytia, protein and RNA abundance, and fluorescent signal were compared between groups by using a generalized linear model (MIXED procedure) that allows adjustment of means considering the time effect. The model used included treatment groups and time as fixed effects. Data were tested for normality by the Anderson-Darling normality test. LSMEANS were used to adjust the means and to compare treatments. Significance was set at $p < 0.05$. All data were analyzed using SAS (version 9.4; SAS Institute Inc.).

Results

BPS/EGFR Competitive Binding Assay

To investigate whether the ability of BPS to block EGFR phosphorylation is via interference with natural ligand binding, a competitive EGFR binding assay was performed (Figure 1). The alpha signal was significantly lower when biotinylated EGF was co-exposed with anti-EGF or anti-EGFR (cetuximab) antibodies ($p < 0.05$). BPS significantly blocked the tagged EGF binding in a dose-dependent manner, reducing the alpha signal by 15%, 46%, and 54% for doses of 0.1, 1, and 10 µg/mL of BPS, respectively ($p < 0.05$). The calculated EC_{50} for BPS competitive binding was 0.2 µg/mL. The DMSO vehicle control group did not alter the alpha signal.

BPS Effects on EGFR Phosphorylation

To evaluate whether BPS can block EGFR phosphorylation, we used the MDA-MD-231 breast cancer cell line. Exposure of MDA-MD-231 cells to EGF for 15 min led to >110-fold up-regulation of p-EGFR compared with the control group ($p = 0.004$, Figure 2) when normalized to total EGFR expression, with no effect when cells were exposed to BPS alone. EGF-stimulated p-EGFR was 41.3-fold lower when co-exposed to EGF + BPS ($p = 0.006$). EGF up-regulated p-AKT by 9.5-fold when normalized to total AKT expression ($p < 0.001$). However,

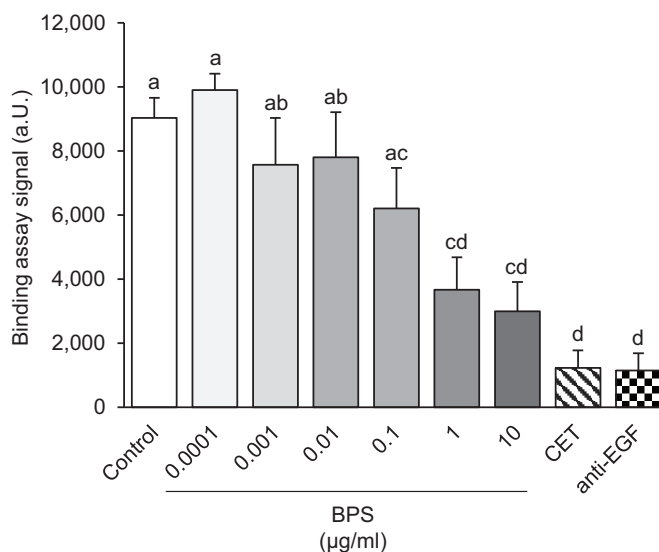


Figure 1. EGFR competitive binding assay. Binding signal (mean ± SEM) in alpha units (a.u.) after exposure to BPS at a range of doses from 0.0001 to 10 µg/mL. Both positive controls, cetuximab (CET) and anti-EGF antibody, were used at 0.1 µg/mL ($n = 5$ replicates/group). A generalized linear model was used to compare treatments. Different letters denote statistical differences among treatment groups at $p < 0.05$. Note: BPS, bisphenol S; CET, cetuximab; EGF, epidermal growth factor; EGFR, EGF receptor; SEM, standard error of the mean.

the EGF-induced up-regulation of p-AKT was not attenuated when MDA-MD-231 cells were co-exposed with EGF + BPS ($p = 0.66$). To further confirm the ability of BPS to block p-EGFR, we assessed the level of EGFR phosphorylation through immunocytochemistry in hCTB cells co-exposed to EGF + BPS (Figure 3). The phosphorylation level of EGFR was lower when cells were exposed to EGF + BPS vs. EGF alone ($p = 0.006$).

BPS Effects on EGF Internalization

To further confirm that BPS acts as a competitive antagonist, we demonstrated its ability to displace bound fluorescent EGF from the EGFR binding site through a competitive EGF internalization assay. hCTB cells displayed less internalization of Alexa Fluor 647-tagged EGF, in a dose-dependent manner, after exposure to 1 or 10 µg/mL of BPS (Figure 4). When co-exposed with BPS, Alexa Fluor 647-tagged EGF internalization in hCTB cells was 21% ($p = 0.02$) and 43% ($p < 0.01$) lower at 1 and 10 µg/mL of BPS doses, respectively. In MDA-MD-231 cells the Alexa Fluor 647-tagged EGF internalization was 26% lower when cells were co-exposed to 10 µg/mL of BPS ($p = 0.02$; Figure 5).

BPS Effects on hCTB Syncytialization in Vitro

To test whether BPS can affect cytotrophoblast syncytialization, hCTB cells were exposed to 200 ng/mL of BPS for 96 h in the presence or absence of recombinant human EGF. The percentage of syncytia in the BPS-exposed group did not differ from that of the control group (Figure 6). However, BPS blocked EGF-mediated syncytialization ($p < 0.05$) to the level of the vehicle group. None of the BPS or EGF doses used in the study affected hCTB viability (Figure S2).

BPS Effects on EGF-Responsive Genes

To determine the expression of EGF-responsive genes over time, MDA-MD-231 cells were exposed to EGF for 1, 3, 6, and 9 h, and mRNA production of three relevant genes were evaluated.

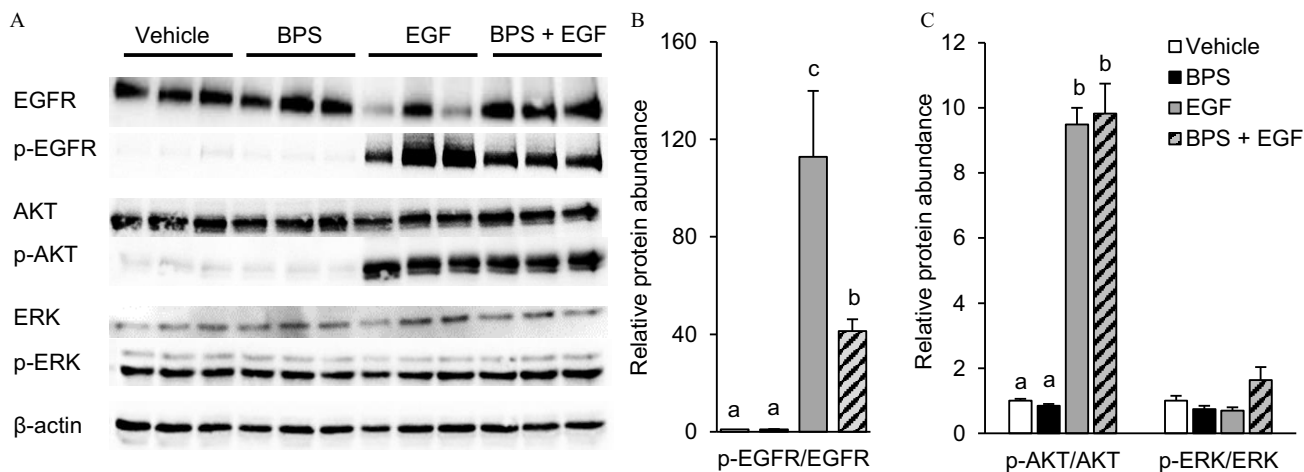


Figure 2. Effect of BPS exposure on EGF-mediated EGFR pathway activation in MDA-MD-231 cells. (A) Representative western blot images for total and phosphorylated proteins and the reference protein β -actin upon exposure to vehicle (0.1% DMSO), BPS (200 ng/mL; black bars), EGF (10 ng/mL; gray bars), or BPS + EGF (stripped bars). (B) p-EGFR and (C) p-AKT and p-ERK protein expression relative to vehicle group (mean \pm SEM). $n = 3$ replicates/group. A generalized linear model was used to compare treatments. Different letters denote statistical differences among treatment groups at $p < 0.05$. Note: BPS, bisphenol S; DMSO, dimethyl sulfoxide; EGF, epidermal growth factor; p-EGFR, phospho-EGF receptor; p-AKT, phospho-protein kinase B; p-ERK, phospho-extracellular receptor kinase; SEM, standard error of the mean.

The maximum response was observed at 1 h to *PTGS2* and at 3 h post exposure to *CCND1* and *MYC* (Figure 7A). Therefore, BPS-dependent inhibition of EGF-mediated gene expression was tested after 3 h in the presence or absence of recombinant human EGF. Gene expression of *MYC* was similar to the control when the cells were co-exposed to EGF + BPS but lower than the EGF group ($p < 0.05$; Figure 7B). No differences were detected in the mRNA expression of *CCND1* and *PTGS2* exposed to BPS.

BPS Effects on Cell Proliferation

To test whether BPS can affect MDA-MD-231 cells proliferation, cells were exposed to BPS in the presence or absence of recombinant human EGF. The proportion of proliferative cells was not significantly different between BPS- and vehicle-exposed cells

(Figure 8). However, BPS blocked EGF-induced proliferation (by $\sim 6\%$; $p < 0.05$) to the level of the vehicle and BPS groups.

Discussion

In the present study, we have shown that BPS, an emerging bisphenol chemical, blocked EGF-mediated cell fusion in primary hCTB cells at the dose of 200 ng/mL of BPS. In support of this, our data showed that BPS *a*) competitively bound to EGFR; *b*) reduced EGFR phosphorylation; and *c*) reduced EGF internalization in hCTB cells. The interference of BPS with EGF-mediated signaling was further demonstrated in MDA-MD-231 cells, a breast adenocarcinoma cell line responsive to EGF. BPS also *a*) prevented EGF-mediated EGFR/ERK signaling through inhibition of EGFR phosphorylation; *b*) reduced EGF internalization; *c*) reduced EGF-mediated *MYC* expression, a transcription factor involved in the regulation of proliferation, mitogenesis, differentiation, and programmed cell death (Hanson et al. 1994); and *d*) dampened EGF-mediated cell proliferation in MDA-MD-231 cells. Overall, these findings indicate that BPS has the potential to disrupt EGF-mediated functions in the placenta (see the proposed working model in Figure 9).

Using an EGF competitive binding assay, our findings suggest that BPS acts as an antagonist by competing with EGF for the EGFR binding site. This finding suggests that BPS interacts with the EGFR extracellular domain, which contains four subdomains (I, II, III, and IV). Importantly, only subdomains I and III are involved in EGF binding (Ogiso et al. 2002). Because BPS competes with EGF for EGFR binding, we further hypothesized that the binding site for BPS should overlap, at least partially, with the natural ligand binding site on subdomains I and/or III. BPS binding to these subdomains is also consistent with the ability of BPS to inhibit EGFR downstream signaling, as shown by EGFR phosphorylation and *MYC* expression. EGFR is a cell surface receptor that presents in either an inactive or active conformation. When inactive, subdomains II and IV are tethered, and subdomains I and III are positioned too far apart for EGF to bind simultaneously to both subdomains. In the active conformation, subdomain I becomes available for ligand co-binding with subdomain III, causing the activation of EGFR's intrinsic protein tyrosine kinase activity and autophosphorylation (Ferguson 2004). Given that binding to both subdomains results in

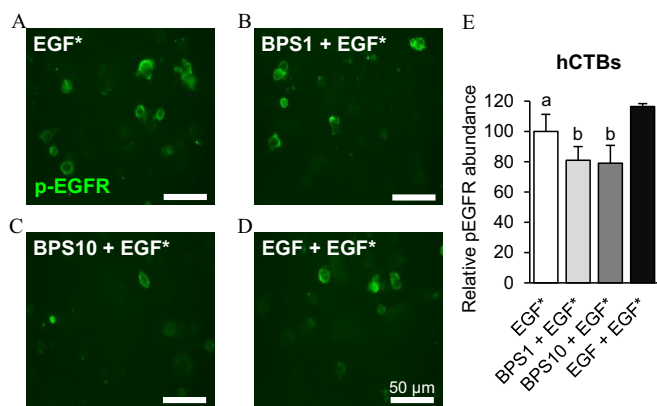


Figure 3. Effect of BPS on p-EGFR in human cytotrophoblasts (hCTBs). (A–D) Representative images and (E) quantification of p-EGFR (mean \pm SEM) of hCTBs immunostained against p-EGFR following exposure to EGF* (100 ng/mL Alexa Fluor 647-labeled EGF) (A); BPS1 + EGF* (1 μ g/mL BPS + 100 ng/mL EGF*) (B); BPS10 + EGF* (10 μ g/mL BPS + 100 ng/mL EGF*) (C); and EGF + EGF* (100 ng/mL nonlabeled EGF + 100 ng/mL EGF*) (D). Images were taken 1 h after a 5-min exposure. $n = 3$ replicates/group. A generalized linear model was used to compare treatments. Different letters denote statistical differences among treatment groups at $p < 0.05$. Note: BPS, bisphenol S; EGF, epidermal growth factor; p-EGFR, phospho-EGF receptor; SEM, standard error of the mean.

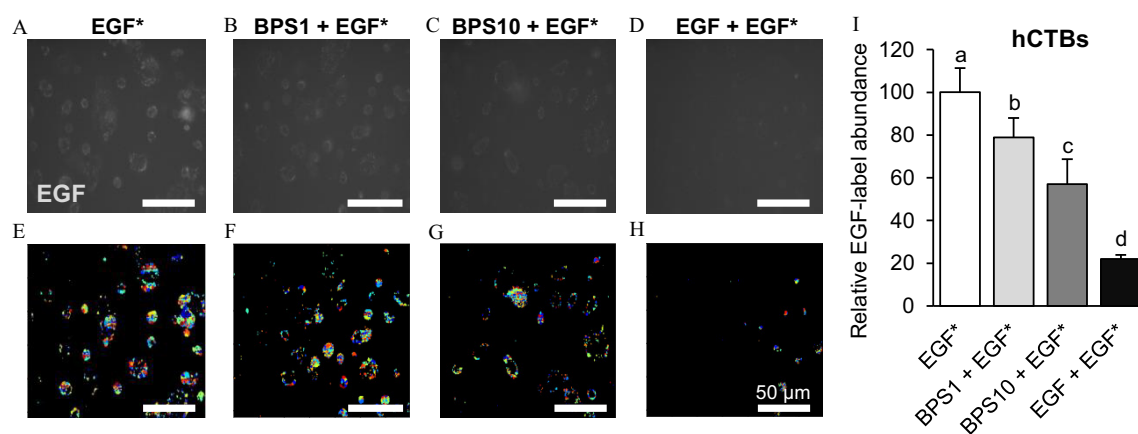


Figure 4. Effect of BPS on EGF internalization in human cytotrophoblasts (hCTBs). (A–D) Representative images of EGF in hCTBs, (E–H) their respective post-processed images, and (I) quantification (mean \pm SEM) following exposure to EGF* (100 ng/Alexa Fluor 647-labeled EGF) (A,E); BPS1 + EGF* (1 μ g/mL BPS + 100 ng/mL EGF*) (B,F); BPS10 + EGF* (10 μ g/mL BPS + 100 ng/mL EGF*) (C,G); and EGF + EGF* (100 ng/mL nonlabeled EGF + 100 ng/mL EGF*) (D,H). Images were taken 1 h after a 5-min exposure. The results were normalized by the number of cells and are expressed as the percentage of the EGF* group. $n = 4$ replicates/group. A generalized linear model was used to compare treatments. Different letters denote statistical differences among treatment groups at $p < 0.05$. Colors in the processed images indicate the individual fluorescent signals detected by the software used to quantify the EGF internalization. Note: BPS, bisphenol S; EGF, epidermal growth factor; SEM, standard error of the mean.

stimulation of EGFR activity (Mi et al. 2011) and exposure to BPS results in lower levels of EGFR phosphorylation and EGF internalization, BPS likely binds EGFR in just one subdomain. Other EDCs, such as polychlorinated biphenyl congener-126 (PCB-126) and PCB-153 have been reported to be EGFR antagonists (Hardesty et al. 2018). These PCBs were predicted to bind EGFR in a congener-specific manner, with PCB-126 predicted to bind within a hydrophobic pocket of subdomain III and PCB-153 predicted to bind within a hydrophobic pocket between subdomains II and IV. To our knowledge, there are no studies investigating whether these chemicals interfere with EGFR-mediated trophoblast fusion. Future *in silico* studies will be necessary to determine the specific EGFR binding site of BPS.

The competitive antagonism of BPS to EGFR was further supported by its ability to reduce EGFR phosphorylation in a breast adenocarcinoma cells and in primary isolated hCTBs. In addition, lower EGFR expression was observed when cells were exposed to EGF. This was possibly due a rapid receptor protein degradation after phosphorylation. However, degradation of

EGFR was not evident by BPS when co-exposed to EGF + BPS. This could be due the lower level of phosphorylated EGFR or reduced EGFR degradation in the presence of BPS. Similar to BPS, other chemicals like chlordane, *trans*-nonachlor, PCBs, and atrazine can also block EGFR phosphorylation in HepG2 cells (Hardesty et al. 2018). However, their direct effect on placental syncytialization has not been demonstrated. Interestingly, diminished placental EGFR phosphorylation has been observed in women exposed to higher levels of PCBs (Hardesty et al. 2017), positively correlated with lower birth weights (Lucier et al. 1987), and known to be associated with placental dysfunction (Naeye 1987). The ability of BPS to block EGFR phosphorylation can also result in decreased signaling for multiple cellular pathways activated by EGFR important to syncytialization in trophoblast cells including MAPK and janus kinase/signal transducer and activator of transcription (Gupta et al. 2016).

Our experimental design allowed us to track the magnitude of the EGFR signal inhibition. EGFR has four sequential and highly regulated steps for activation: a) EGF binding to an inactive

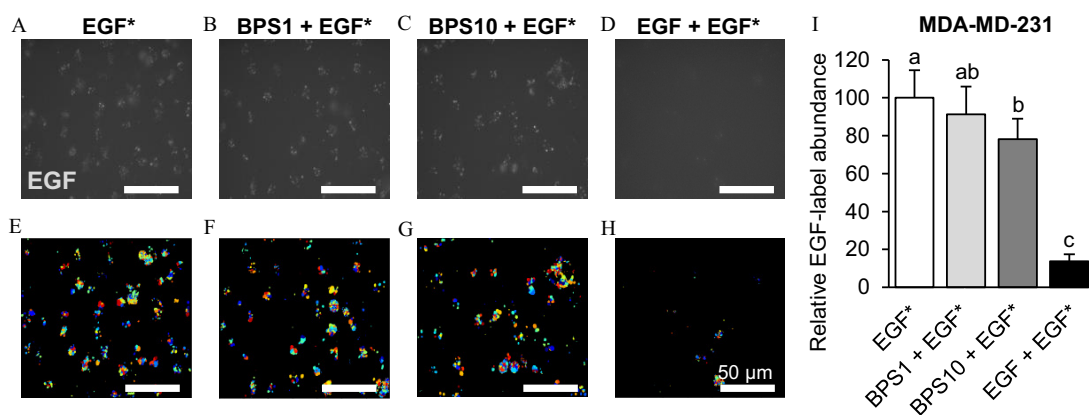


Figure 5. Effect of BPS on EGF internalization in MDA-MD-231 cells. (A–D) Representative images of EGF in MDA-MD-231 cells, (E–H) their respective post-processed images, and (I) quantification (mean \pm SEM) following exposure to EGF* (100 ng/Alexa Fluor 647-labeled EGF) (A,E); BPS1 + EGF* (1 μ g/mL BPS + 100 ng/mL EGF*) (B,F); BPS10 + EGF* (10 μ g/mL BPS + 100 ng/mL EGF*) (C,G); and EGF + EGF* (100 ng/mL nonlabeled EGF + 100 ng/mL EGF*) (D,H). Images were taken 1 h after a 5-min exposure. The results were normalized by the number of cells and are expressed as the percentage of the EGF* group. $n = 4$ replicates/group. A generalized linear model was used to compare treatments. Different letters denote statistical differences among treatment groups at $p < 0.05$. Colors in the processed images indicate the individual fluorescent signals detected by the software used to quantify the EGF internalization. Note: BPS, bisphenol S; EGF, epidermal growth factor; SEM, standard error of the mean.

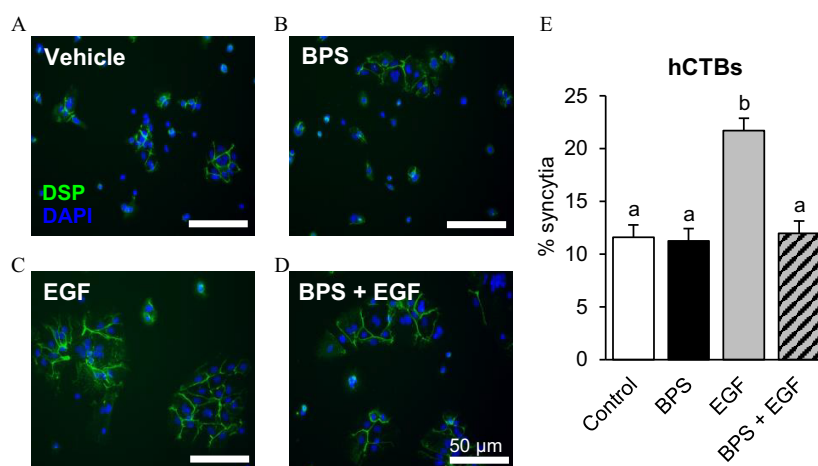


Figure 6. Effect of BPS exposure on human cytotrophoblast (hCTB) syncytialization. Representative images of hCTBs immunostained against desmoplakin (DSP; green) following a 96-h exposure to (A) vehicle (0.1% DMSO), (B) BPS (200 ng/mL), (C) EGF (10 ng/mL), or (D) BPS + EGF. Nuclei were stained with DAPI (blue). (E) The percentage of syncytia [percentage of cells forming a syncytia (≥ 3 nuclei)] is represented as mean \pm SEM. $n = 6$ primary hCTB cell cultures/group. A generalized linear model was used to compare treatments. Different letters denote statistical differences among treatment groups at $p < 0.05$. Note: BPS, bisphenol S; DAPI, 4',6-diamidino-2-phenylindole; DMSO, dimethyl sulfoxide; EGF, epidermal growth factor; SEM, standard error of the mean.

EGFR monomer generating an active monomer; *b*) homo- or heterodimerization of ligand-bound monomers; *c*) autophosphorylation of the tyrosine kinase domain; and *d*) endocytosis and internalization of EGF-bound EGFRs (Citri and Yarden 2006). We have demonstrated that exposure to BPS results in lower EGF internalization in MDA-MD-231 cells and in primary isolated hCTBs, reinforcing the premise that BPS acts as an EGFR antagonist and competes with EGF for EGFR binding. Importantly, the magnitude of this effect was greater in hCTB cells. Given that resistance to EGFR inhibitors occurs primarily upon chronic exposures (You et al. 2018), the higher abundance of EGFR in placental cells (Filla and Kaul 1997) may underline the stronger response observed in hCTBs upon BPS exposure. A similar inhibition of EGF internalization and EGFR phosphorylation has been reported for PCB-126, PCB-153, and *trans*-nonachlor in a human epidermoid carcinoma cell line (Hardesty et al. 2018) although their direct effect on placental syncytialization has not been demonstrated. Internalized EGFR can be recycled or

undergo lysosomal degradation, making the study of EGFR internalization challenging. EGFR recycling appears to be the default mechanism where endosomes are formed, and lysosomal degradation is used to attenuate EGFR signaling (Roepstorff et al. 2008). Whether BPS alters how EGFR is internalized needs to be further investigated. Reduced EGFR internalization can reduce EGFR recycling back to the cell surface. This lack of recycling may reduce the overall EGFR downstream signal, in turn compromising EGF-mediated processes in the placenta, such as trophoblast syncytialization.

We have demonstrated that BPS blocks EGFR signaling in human primary cytotrophoblast cells. This is critical because the placenta is one of the tissues with the highest EGFR expression (Filla and Kaul 1997) and, more importantly, EGF is required for cytotrophoblast cell fusion (Filla and Kaul 1997). The fact that BPS fully attenuated EGF-mediated fusion in primary hCTBs has important implications in human pregnancies because pregnancy complications such as preeclampsia and intrauterine growth

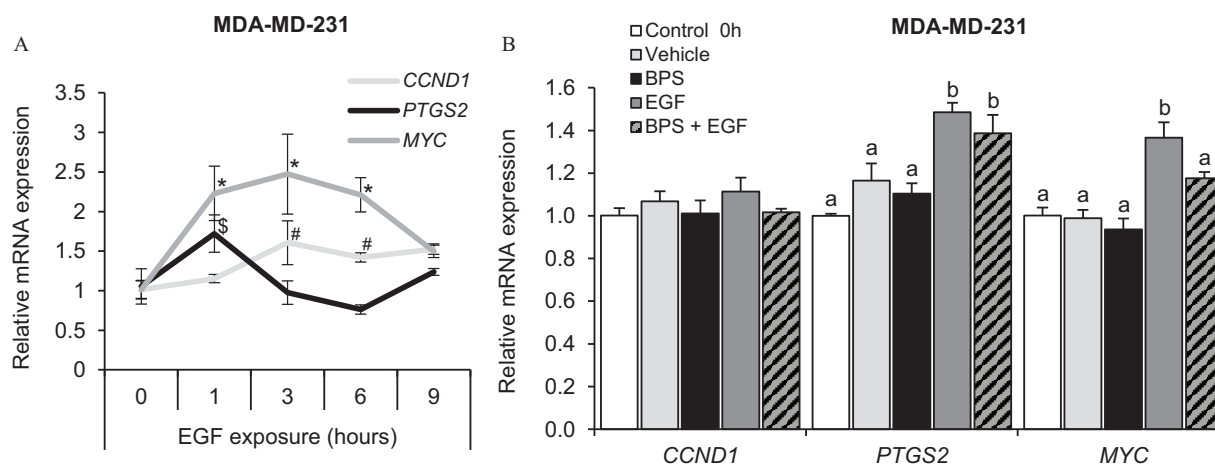


Figure 7. Effect of BPS exposure on the EGFR-responsive genes of MDA-MD-231 cells. (A) Relative EGFR-responsive gene expression (mean \pm SEM) on MDA-MD-231 cells exposed to 10 ng/mL of EGF for 1, 3, 6, and 9 h. A generalized linear model was used to compare treatments. *, \$, and # denote statistical differences from 0 h within *MYC*, *PTGS2*, and *CCND1* genes, respectively. (B) Relative EGFR-responsive gene expression (mean \pm SEM) in MDA-MD-231 cells after 0-h (control; no exposure) or 3-h exposure to vehicle (0.1% DMSO), EGF (10 ng/mL), BPS (200 ng/mL), or BPS + EGF (same doses as single groups). $n = 3$ /group. A generalized linear model was used to compare treatments. Different letters denote statistical differences among treatment groups at $p < 0.05$. Note: BPS, bisphenol S; *CCND1*, cyclin D1 gene; DMSO, dimethyl sulfoxide; EGF, epidermal growth factor; EGFR, EGF receptor; *MYC*, MYC proto-oncogene; *PTGS2*, prostaglandin-endoperoxide synthase gene; SEM, standard error of the mean.

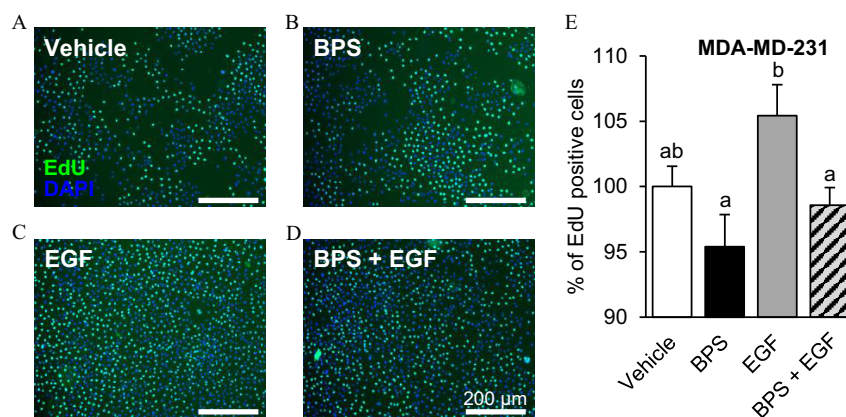


Figure 8. Effect of BPS exposure on the proliferation of MDA-MD-231 cells. (A–D) Representative images of MDA-MD-231 cells exposed to 5-ethynyl-2'-deoxyuridine (EdU; 10 μ M) for 3 h (EdU-positive, green). Nuclei were stained with DAPI (blue) following 72-h exposure to vehicle (0.1% DMSO) (A); BPS (200 ng/mL) (B); EGF (10 ng/mL) (C); or BPS + EGF (D) (same doses as single groups). (E) Cell proliferation (mean \pm SEM) was expressed as the percentage of EdU-positive cells of the total number of nuclei and normalized to the vehicle group. $n = 3$ /group. A generalized linear model was used to compare treatments. Different letters denote statistical differences among treatment groups at $p < 0.05$. Note: BPS, bisphenol S; DAPI, 4',6-diamidino-2-phenylindole; DMSO, dimethyl sulfoxide; EGF, epidermal growth factor; SEM, standard error of the mean.

restriction have been associated with impaired syncytialization and reduced STB layer formation (Langbein et al. 2008). Given that BPS is commonly used in the manufacturing of epoxy glues, food can coatings, thermal receipt papers, textile dyes, and tanning agents (Chen 2016), over 80% of the population is routinely exposed to it (Liao et al. 2012a). The BPS concentration used in this study is within the upper limit of the urinary BPS concentration range in the general U.S. population [0.07–211.9 ng/mL (NHANES 2016)]. Information regarding circulating concentrations of BPS in maternal blood, fetal, or placental tissues remains scarce. Similar to BPA, BPS is likely to be two to three magnitudes lower in fetal and placental tissues compared with that at the higher end of urinary concentrations (Lee et al. 2018). To note, BPS is being used as a replacement chemical in thermal paper

(ECHA 2020), indicating that, like BPA (Hehn 2016) occupational exposure levels to BPS will continue to increase (Ndaw et al. 2018) and likely surpass those currently observed for BPA (Hehn 2016). Our group has demonstrated that BPS exposures of as low as 100 ng/mL BPS can alter gap junction intercellular communication in steroidogenic ovarian theca cells (Gingrich 2020). Follow-up dose–response studies are necessary to determine the effect of low-dose BPS exposure on EGFR phosphorylation and downstream signaling.

Conclusion

To our knowledge, this is the first study to demonstrate that BPS can act as a competitive antagonist to EGFR, blocking EGF

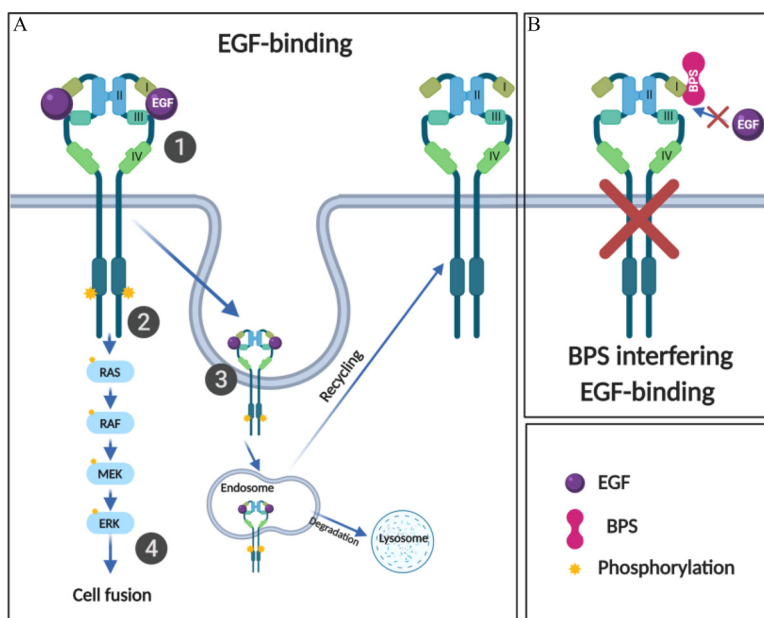


Figure 9. Working model of the interference of BPS with the EGFR pathway. (A, Step 1) Upon EGF binding to EGFR on domains I and III, (Step 2) EGFR autophosphorylates the tyrosine kinase domain, and (Step 3) recruits proteins at the intracellular portion of the receptors to enable EGFR/EGF endocytosis. The internalized EGFR can be sorted both for recycling and for lysosomal degradation. (Step 4) Activation of EGFR pathway induces cell fusion in human cytotrophoblasts. (B) In the presence of BPS, EGF is blocked from binding to EGFR, blocking EGFR phosphorylation and pathway activation. Note: BPS, bisphenol S; EGF, epidermal growth factor; EGFR, EGF receptor; ERK, extracellular signal-regulated kinase; MEK, mitogen-activated protein kinase; RAF, rapidly accelerated fibrosarcoma kinase; RAS, rat sarcoma signaling molecule.

internalization and EGFR phosphorylation in human placental cytotrophoblast and triple-negative breast cancer cell lines. This effect was achieved at a dose within the range observed in human urinary concentrations. Importantly, BPS can prevent EGF-mediated cytotrophoblast syncytialization. Given the role of EGFR in placental development, including cytotrophoblast proliferation, differentiation, and fusion, gestational BPS exposure may result in placenta dysfunction.

Acknowledgments

We thank S.K. Kshirsagar for her help in human cytotrophoblast isolation training. This work was supported by the National Institutes of Health (NIH)/National Institute of Environmental Health Sciences (R01ES027863 to A.V.-L.) and the *Eunice Kennedy Shriver* National Institute of Child Health and Human Development (NICHD; R21HD083058 to M.G.P.). J.G. was supported in part by NICHD under award number T32HD087166. The content is solely the responsibility of the authors and does not necessarily represent the official views of the NIH.

References

- Chen D, Kannan K, Tan H, Zheng Z, Feng YL, Wu Y, et al. 2016. Bisphenol analogues other than BPA: environmental occurrence, human exposure, and toxicity—a review. *Environ Sci Technol* 50(11):5438–5453, PMID: 27143250, <https://doi.org/10.1021/acs.est.5b05387>.
- Citri A, Yarden Y. 2006. EGF-ERBB signalling: towards the systems level. *Nat Rev Mol Cell Biol* 7(7):505–516, PMID: 16829981, <https://doi.org/10.1038/nrm1962>.
- Dackor J, Strunk KE, Wehmeyer MM, Threadgill DW. 2007. Altered trophoblast proliferation is insufficient to account for placental dysfunction in *Egfr* null embryos. *Placenta* 28(11–12):1211–1218, PMID: 17822758, <https://doi.org/10.1016/j.placenta.2007.07.005>.
- Diamanti-Kandarakis E, Bourguignon JP, Giudice LC, Hauser R, Prins GS, Soto AM, et al. 2009. Endocrine-disrupting chemicals: an endocrine society scientific statement. *Endocr Rev* 30(4):293–342, PMID: 19502515, <https://doi.org/10.1210/er.2009-0002>.
- ECHA (European Chemicals Agency). 2020. *The Use of bisphenol A and Its Alternatives in Thermal Paper in the EU during 2014–2022*. Helsinki, Finland: European Chemicals Agency. https://www.echa.europa.eu/documents/10162/23294236/bpa_thermal_paper_report_2020_en.pdf [accessed 29 January 2021].
- Faxén M, Nasiell J, Blanck A, Nisell H, Lunell NO. 1998. Altered mRNA expression pattern of placental epidermal growth factor receptor (EGFR) in pregnancies complicated by preeclampsia and/or intrauterine growth retardation. *Am J Perinatol* 15(1):9–13, PMID: 9475680, <https://doi.org/10.1055/s-2007-993890>.
- Ferguson KM. 2004. Active and inactive conformations of the epidermal growth factor receptor. *Biochem Soc Trans* 32(pt 5):742–745, PMID: 15494003, <https://doi.org/10.1042/BST0320742>.
- Filla MS, Kaul KL. 1997. Relative expression of epidermal growth factor receptor in placental cytotrophoblasts and choriocarcinoma cell lines. *Placenta* 18(1):17–27, PMID: 9032806, [https://doi.org/10.1016/s0143-4004\(97\)90067-9](https://doi.org/10.1016/s0143-4004(97)90067-9).
- Fowden AL, Moore T. 2012. Maternal-fetal resource allocation: co-operation and conflict. *Placenta* 33(suppl 2):e11–e15, PMID: 22652046, <https://doi.org/10.1016/j.placenta.2012.05.002>.
- Fujii T, Nagamatsu T, Morita K, Schust DJ, Iriyama T, Komatsu A, et al. 2017. Enhanced HIF2 α expression during human trophoblast differentiation into syncytiotrophoblast suppresses transcription of placental growth factor. *Sci Rep* 7(1):12455, PMID: 28963486, <https://doi.org/10.1038/s41598-017-12685-w>.
- Gingrich J, Pu Y, Roberts J, Karthikraj R, Kannan K, Ehrhardt R, et al. 2018. Gestational bisphenol S impairs placental endocrine function and the fusogenic trophoblast signaling pathway. *Arch Toxicol* 92(5):1861–1876, PMID: 29550860, <https://doi.org/10.1007/s00204-018-2191-2>.
- Gingrich J, Pu Y, Upham B, Veiga-Lopez A. 2020. Bisphenol-specific effects on gap junction intercellular communication in ovarian theca cells [Abstract]. *Toxicologist* 150(10):1777.
- Gore AC, Chappell VA, Fenton SE, Flaws JA, Nadal A, Prins GS, et al. 2015. EDC-2: the Endocrine Society's second Scientific Statement on endocrine-disrupting chemicals. *Endocr Rev* 36(6):E1–E150, PMID: 26544531, <https://doi.org/10.1210/er.2015-1010>.
- Gupta SK, Malhotra SS, Malik A, Verma S, Chaudhary P. 2016. Cell signaling pathways involved during invasion and syncytialization of trophoblast cells. *Am J Reprod Immunol* 75(3):361–371, PMID: 26490782, <https://doi.org/10.1111/aji.12436>.
- Hanson KD, Shichiri M, Follansbee MR, Sedivy JM. 1994. Effects of c-myc expression on cell cycle progression. *Mol Cell Biol* 14(9):5748–5755, PMID: 8065309, <https://doi.org/10.1128/mcb.14.9.5748>.
- Hardesty JE, Al-Eryani L, Wahlang B, Falkner KC, Shi H, Jin J, et al. 2018. Epidermal growth factor receptor signaling disruption by endocrine and metabolic disrupting chemicals. *Toxicol Sci* 162(2):622–634, PMID: 29329451, <https://doi.org/10.1093/toxsci/kfy004>.
- Hardesty JE, Wahlang B, Falkner KC, Clair HB, Clark BJ, Ceresa BP, et al. 2017. Polychlorinated biphenyls disrupt hepatic epidermal growth factor receptor signaling. *Xenobiotica* 47(9):807–820, PMID: 27458090, <https://doi.org/10.1080/00498254.2016.1217572>.
- Hehn RS. 2016. NHANES data support link between handling of thermal paper receipts and increased urinary bisphenol A excretion. *Environ Sci Technol* 50(1):397–404, PMID: 26583963, <https://doi.org/10.1021/acs.est.5b04059>.
- Hill CE, Sapouckey SA, Suvorov A, Vandenberg LN. 2017. Developmental exposures to bisphenol S, a BPA replacement, alter estrogen-responsiveness of the female reproductive tract: a pilot study. *Cogent Med* 4:1317690, PMID: 31231671, <https://doi.org/10.1080/2331205X.2017.1317690>.
- Holets LM, Carletti MZ, Kshirsagar SK, Christenson LK, Petroff MG. 2009. Differentiation-induced post-transcriptional control of B7-H1 in human trophoblast cells. *Placenta* 30(1):48–55, PMID: 19010538, <https://doi.org/10.1016/j.placenta.2008.10.001>.
- Jing J, Pu Y, Gingrich J, Veiga-Lopez A. 2019. Gestational exposure to bisphenol A and bisphenol S leads to fetal skeletal muscle hypertrophy independent of sex. *Toxicol Sci* 172(2):292–302, PMID: 31501865, <https://doi.org/10.1093/toxsci/kfz198>.
- Kang DY, Sp N, Kim DH, Joung YH, Lee HG, Park YM, et al. 2018. Salidroside inhibits migration, invasion and angiogenesis of MDA-MB 231 TNBC cells by regulating EGFR/Jak2/STAT3 signaling via MMP2. *Int J Oncol* 53(2):877–885, PMID: 29901185, <https://doi.org/10.3892/ijo.2018.4430>.
- Kinch CD, Ibhazehiebo K, Jeong JH, Habibi HR, Kurrasch DM. 2015. Low-dose exposure to bisphenol A and replacement bisphenol S induces precocious hypothalamic neurogenesis in embryonic zebrafish. *Proc Natl Acad Sci USA* 112(5):1475–1480, PMID: 25583509, <https://doi.org/10.1073/pnas.1417731112>.
- Kliman HJ, Nestler JE, Sermasi E, Sanger JM, Strauss JF III. 1986. Purification, characterization, and *in vitro* differentiation of cytotrophoblasts from human term placentae. *Endocrinology* 118(4):1567–1582, PMID: 3512258, <https://doi.org/10.1210/endo-118-4-1567>.
- Langbein M, Strick R, Strissel PL, Vogt N, Parsch H, Beckmann MW, et al. 2008. Impaired cytotrophoblast cell–cell fusion is associated with reduced Syncytin and increased apoptosis in patients with placental dysfunction. *Mol Reprod Dev* 75(1):175–183, PMID: 17546632, <https://doi.org/10.1002/mrd.20729>.
- Lee J, Choi K, Park J, Moon HB, Choi G, Lee JJ, et al. 2018. Bisphenol A distribution in serum, urine, placenta, breast milk, and umbilical cord serum in a birth panel of mother–neonate pairs. *Sci Total Environ* 626:1495–1501, PMID: 29146078, <https://doi.org/10.1016/j.scitotenv.2017.10.042>.
- Liao C, Kannan K. 2013. Concentrations and profiles of bisphenol A and other bisphenol analogues in foodstuffs from the United States and their implications for human exposure. *J Agric Food Chem* 61(19):4655–4662, PMID: 23614805, <https://doi.org/10.1021/jf400445n>.
- Liao C, Liu F, Alomirah H, Loi VD, Mohd MA, Moon HB, et al. 2012a. Bisphenol S in urine from the United States and seven Asian countries: occurrence and human exposures. *Environ Sci Technol* 46(12):6860–6866, PMID: 22620267, <https://doi.org/10.1021/es301334j>.
- Liao C, Liu F, Guo Y, Moon HB, Nakata H, Wu Q, et al. 2012b. Occurrence of eight bisphenol analogues in indoor dust from the United States and several Asian countries: implications for human exposure. *Environ Sci Technol* 46(16):9138–9145, PMID: 22784190, <https://doi.org/10.1021/es302004w>.
- Liao C, Liu F, Moon HB, Yamashita N, Yun S, Kannan K. 2012c. Bisphenol analogues in sediments from industrialized areas in the United States, Japan, and Korea: spatial and temporal distributions. *Environ Sci Technol* 46(21):11558–11565, PMID: 23020513, <https://doi.org/10.1021/es303191g>.
- Lucier GW, Nelson KG, Everson RB, Wong TK, Philpot RM, Tiernan T, et al. 1987. Placental markers of human exposure to polychlorinated biphenyls and polychlorinated dibenzofurans. *Environ Health Perspect* 76:79–87, PMID: 2834196, <https://doi.org/10.1289/ehp.877679>.
- Malassiné A, Cronier L. 2002. Hormones and human trophoblast differentiation: a review. *Endocrine* 19(1):3–11, PMID: 12583598, <https://doi.org/10.1385/ENDO:19:1:3>.
- Maruo T, Matsuo H, Murata K, Mochizuki M. 1992. Gestational age-dependent dual action of epidermal growth factor on human placenta early in gestation. *J Clin Endocrinol Metab* 75(5):1362–1367, PMID: 1430098, <https://doi.org/10.1210/jcem.75.5.1430098>.
- McQuin C, Goodman A, Chernyshev V, Kametsky L, Cimini BA, Karhohs KW, et al. 2018. CellProfiler 3.0: next-generation image processing for biology. *PLoS Biol* 16(7):e2005970, PMID: 29969450, <https://doi.org/10.1371/journal.pbio.2005970>.

- Mi LZ, Lu C, Li Z, Nishida N, Walz T, Springer TA. 2011. Simultaneous visualization of the extracellular and cytoplasmic domains of the epidermal growth factor receptor. *Nat Struct Mol Biol* 18(9):984–989, PMID: 21822280, <https://doi.org/10.1038/nsmb.2092>.
- Naeye RL. 1987. Functionally important disorders of the placenta, umbilical cord, and fetal membranes. *Hum Pathol* 18(7):680–691, PMID: 3297994, [https://doi.org/10.1016/s0046-8177\(87\)80239-3](https://doi.org/10.1016/s0046-8177(87)80239-3).
- Ndaw S, Remy A, Denis F, Marsan P, Jargot D, Robert A. 2018. Occupational exposure of cashiers to bisphenol S via thermal paper. *Toxicol Lett* 298:106–111, PMID: 29800715, <https://doi.org/10.1016/j.toxlet.2018.05.026>.
- NHANES (National Health and Nutrition Examination Survey). 2016. 2013–2014 Data Documentation, Codebook, and Frequencies. Personal Care and Consumer Product Chemicals and Metablit (EPHPP_H). Data file: EPHPP-H.xpt. Last revised: September 2016. https://www.cdc.gov/Nchs/Nhanes/2013-2014/EPHPP_H.htm [accessed 29 January 2021].
- Ogiso H, Ishitani R, Nureki O, Fukai S, Yamanaka M, Kim JH, et al. 2002. Crystal structure of the complex of human epidermal growth factor and receptor extracellular domains. *Cell* 110(6):775–787, PMID: 12297050, [https://doi.org/10.1016/s0092-8674\(02\)00963-7](https://doi.org/10.1016/s0092-8674(02)00963-7).
- Petroff MG, Phillips TA, Ka H, Pace JL, Hunt JS. 2006. Isolation and culture of term human trophoblast cells. *Methods Mol Med* 121:203–217, PMID: 16251745, <https://doi.org/10.1385/1-59259-983-4-201>.
- Pötgens AJ, Gaus G, Frank HG, Kaufmann P. 2001. Characterization of trophoblast cell isolations by a modified flow cytometry assay. *Placenta* 22(2–3):251–255, PMID: 11170831, <https://doi.org/10.1053/plac.2000.0597>.
- Pu Y, Pearl S, Gingrich J, Jing J, Martin D, Murga-Zamalloa CA, et al. 2019. Multispecies study: low-dose tributyltin impairs ovarian theca cell cholesterol homeostasis through the RXR pathway in five mammalian species including humans. *Arch Toxicol* 93(6):1665–1677, PMID: 31006824, <https://doi.org/10.1007/s00204-019-02449-y>.
- Qiu W, Zhao Y, Yang M, Farajzadeh M, Pan C, Wayne NL. 2016. Actions of bisphenol A and bisphenol S on the reproductive neuroendocrine system during early development in zebrafish. *Endocrinology* 157(2):636–647, PMID: 26653335, <https://doi.org/10.1210/en.2015-1785>.
- Rocha BA, Azevedo LF, Gallimberti M, Campiglia AD, Barbosa F Jr. 2015. High levels of bisphenol A and bisphenol S in Brazilian thermal paper receipts and estimation of daily exposure. *J Toxicol Environ Health A* 78(18):1181–1188, PMID: 26407846, <https://doi.org/10.1080/15287394.2015.1083519>.
- Roepstorff K, Grøvdal L, Grandal M, Lerdrup M, van Deurs B. 2008. Endocytic downregulation of ErbB receptors: mechanisms and relevance in cancer. *Histochem Cell Biol* 129(5):563–578, PMID: 18288481, <https://doi.org/10.1007/s00418-008-0401-3>.
- Schneider CA, Rasband WS, Eliceiri KW. 2012. NIH image to ImageJ: 25 years of image analysis. *Nat Methods* 9(7):671–675, PMID: 22930834, <https://doi.org/10.1038/nmeth.2089>.
- Seravalli V, Di Tommaso M, Challis J, Petraglia F. 2020. Endocrinology of maternal-placental axis. In: *Female Reproductive Dysfunction*. Petraglia F, Fauser B, eds. Cham, Switzerland: Springer, 1–14.
- Tseng JJ, Hsu SL, Wen MC, Ho ESC, Chou MM. 2004. Expression of epidermal growth factor receptor and c-erbB-2 oncoprotein in trophoblast populations of placenta accreta. *Am J Obstet Gynecol* 191(6):2106–2113, PMID: 15592299, <https://doi.org/10.1016/j.ajog.2004.04.043>.
- U.S. EPA (U.S. Environmental Protection Agency). 2016. Assessing and managing chemicals under TSCA. Risk management for bisphenol A (BPA). <https://www.epa.gov/assessing-and-managing-chemicals-under-tsca/risk-management-bisphenol-bpa> [accessed 29 January 2021].
- Uhlén M, Fagerberg L, Hallström BM, Lindskog C, Oksvold P, Mardinoglu A, et al. 2015. Proteomics. Tissue-based map of the human proteome. *Science* 347(6220):1260419, PMID: 25613900, <https://doi.org/10.1126/science.1260419>.
- Wong F, Cox BJ. 2017. Cellular analysis of trophoblast and placenta. *Placenta* 59(suppl 1):S2–S7, PMID: 27932033, <https://doi.org/10.1016/j.placenta.2016.11.015>.
- Yamazaki E, Yamashita N, Taniyasu S, Lam J, Lam PKS, Moon HB, et al. 2015. Bisphenol A and other bisphenol analogues including BPS and BPF in surface water samples from Japan, China, Korea and India. *Ecotoxicol Environ Saf* 122:565–572, PMID: 26436777, <https://doi.org/10.1016/j.ecoenv.2015.09.029>.
- You KS, Yi YW, Kwak SJ, Seong YS. 2018. Inhibition of RPTOR overcomes resistance to EGFR inhibition in triple-negative breast cancer cells. *Int J Oncol* 52(3):828–840, PMID: 29344641, <https://doi.org/10.3892/ijo.2018.4244>.
- Yu JK, Yue CH, Pan YR, Chiu YW, Liu JY, Lin KI, et al. 2018. Isochlorogenic acid C reverses epithelial-mesenchymal transition via down-regulation of EGFR pathway in MDA-MB-231 cells. *Anticancer Res* 38(4):2127–2135, PMID: 29599331, <https://doi.org/10.21873/anticancer.12453>.
- Yu X, Xue J, Yao H, Wu Q, Venkatesan AK, Halden RU, et al. 2015. Occurrence and estrogenic potency of eight bisphenol analogs in sewage sludge from the U.S. EPA targeted national sewage sludge survey. *J Hazard Mater* 299:733–739, PMID: 26298263, <https://doi.org/10.1016/j.jhazmat.2015.07.012>.